

CMRNet++: Map and Camera Agnostic Monocular Visual Localization in LiDAR Maps

Daniele Cattaneo^{1,2}, Domenico Giorgio Sorrenti², Abhinav Valada¹

Abstract—Localization is a critically essential and crucial enabler of autonomous robots. While deep learning has made significant strides in many computer vision tasks, it is still yet to make a sizeable impact on improving capabilities of metric visual localization. One of the major hindrances has been the inability of existing Convolutional Neural Network (CNN)-based pose regression methods to generalize to previously unseen places. Our recently introduced CMRNet effectively addresses this limitation by enabling map independent monocular localization in LiDAR-maps. In this paper, we now take it a step further by introducing CMRNet++ which is a significantly more robust model that not only generalizes to new places effectively, but is also independent of the camera parameters. We enable this capability by moving any metric reasoning outside of the learning process. Extensive evaluations of our proposed CMRNet++ on three challenging autonomous driving datasets namely, KITTI, Argoverse, and Lyft Level5, demonstrate that our network substantially outperforms CMRNet as well as other baselines by a large margin. More importantly, for the first-time, we demonstrate the ability of a deep learning approach to accurately localize without any retraining or fine-tuning in a completely new environment and independent of the camera parameters.

I. INTRODUCTION

Autonomous mobile robots, such as self-driving cars require accurate localization ability to safely navigate in the environment. Although Global Navigation Satellite Systems (GNSSs) provides global positioning, its accuracy and reliability is not adequate for robot navigation. For example, in urban environments, buildings often block or reflect satellites signals that cause non-line-of-sight (NLOS) and multipath issues. In order to alleviate this problem, localization methods that exploit sensors on the robot are used to improve the precision and robustness.

A wide range of methods have been proposed by the research community to tackle this critical localization task using a variety of onboard sensors. While LiDAR-based approaches [1], [2] typically achieve sufficiently accurate localization, their adoption is primarily hindered due to the high cost of these devices. On the other hand, camera-based methods [3]–[5] are more promising for widespread adoption in autonomous vehicles due to the inexpensive sensor cost. Although historically, the performance of camera-based approaches have been subpar compared to LiDAR-based methods, recent advances in computer vision and machine learning have substantially narrowed this gap. Some of these methods that employ CNNs [6]–[10] and random forests [11], [12] directly regress the pose of the camera given a single image. Although these methods have achieved remarkable

results in indoor environments, their performance has been significantly limited in large-scale outdoor environments [13]. Moreover, the biggest caveat is that they can only be employed in locations that these models have been previously trained on.

In the last decade, map providers have been developing the next generation HD maps that are tailored for the automotive domain. These maps include accurate geometric reconstructions of road networks in the form of point clouds generated from LiDARs. This factor has motivated researchers to develop methods that localize a camera inside these LiDAR-maps. Localization can typically be performed by reconstructing the three-dimensional geometry of the scene from a camera, and then matching this reconstruction with the map [14], [15], or by matching in the image plane [16]–[18].

In this paper, we present our CMRNet++ approach for camera to LiDAR-map registration. We build upon our previously proposed CMRNet [18] model that localizes independent of the map, to now also be independent of the camera intrinsics. Unlike existing state-of-the-art CNN-based approaches for pose regression [6], [7], [9], CMRNet does not learn the map, instead it learns to match images to a pre-existing map. Consequently, CMRNet can be used in any environment for which a LiDAR-map is available. However, since the output of CMRNet is metric (a 6-DoF rigid body transformation from an initial pose), the weights of the network are tied to the intrinsic parameters of the camera used for collecting the training data. In this work, we mitigate this problem by decoupling the localization by first employing a pixel to 3D point matching step, followed by a pose regression step. We evaluate our model on KITTI [19], Argoverse [20], and Lyft Level 5 [21] datasets and demonstrate that our approach exceeds state-of-the-art methods while being agnostic to map and camera parameters. Videos showing qualitative results of our approach on each of these datasets are available at <http://rl.uni-freiburg.de/research/vloc-in-lidar>.

II. TECHNICAL APPROACH

We extend CMRNet by decoupling the localization into two phases: a pixel to 3D point matching step, followed by a pose regression step. In the first step, the CNN only focuses on matching at the pixel-level instead of metric basis, which makes the network independent of the intrinsic parameters of the camera. These parameters are instead employed in the second step in which traditional computer vision methods are exploited to estimate the pose of the camera given the matches from the first step. Consequently, after training, CMRNet++ can also be used with different cameras and maps from those used while training. An outline of our proposed CMRNet++ pipeline is depicted in Figure 1.

¹ Department of Computer Science, University of Freiburg, Germany

² Dep. Informatica, Sistemistica e Comunicazione, Università degli studi di Milano - Bicocca, Italy

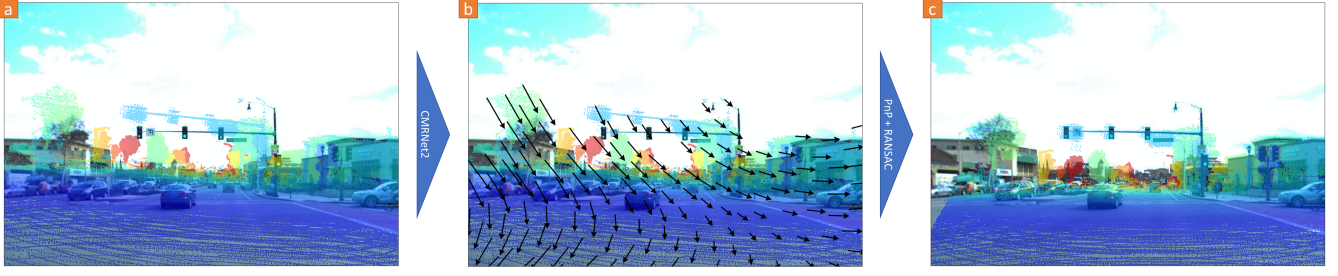


Fig. 1. Outline of the proposed approach. (a) The input LiDAR-image and the RGB image (overlaid for visualization purposes) are fed to our CMRNet++, which predicts (b) pixel displacements between the two inputs. (c) The predicted matches are used to localize the camera using a PnP+RANSAC scheme.

A. Matching Step

For the matching step, we adopt a pipeline similar to CMRNet: starting from an initial pose H_{init} (e.g., obtained from a GNSS), we generate a synthesized depth image that we refer to as a LiDAR-image, by projecting the map into a virtual image plane placed at H_{init} . Figure 1 (a) shows an example of such a LiDAR-image overlaid on the input RGB image. To deal with occlusions in point clouds, we employ a z-buffer technique followed by an occlusion estimation filter. We refer the reader to [18] for more details on this procedure. Once the inputs to our network that consist of the camera image as well as the LiDAR-image have been obtained, for every 3D point in the LiDAR-image, CMRNet++ estimates the pixel of the RGB image that represent the same world point.

The architecture of our proposed CMRNet++ is based on PWC-Net [22] which was introduced for optical flow estimation between two consecutive RGB frames. Unlike PWC-Net, CMRNet++ does not share weights between the two feature pyramid extractors, as the inputs to CMRNet++ are inherently different (RGB image and synthesized depth image). Moreover, since the LiDAR-image only has one channel (i.e., depth), we change the number of input channels of the first convolutional layer in the feature extractor from three to one. The output of CMRNet++ is a dense feature map which is 1/4-th the input resolution and consists of two channels that represent, for every pixel in the LiDAR-image, the displacement (u and v) of the pixel in the RGB image from the same world point. A visual representation of this pixel displacement is depicted in Figure 1 (b).

In order to train CMRNet++, we first need to generate the ground truth pixel displacement ΔP for the aforementioned LiDAR-image to RGB image. To accomplish this, we first compute the coordinates of the map's points in the H_{init} reference frame using Equation (1) and the pixel position of their projection in the LiDAR-image exploiting the intrinsic matrix K of the camera from Equation (2).

$$[\mathbf{x}^{init} \ \mathbf{y}^{init} \ \mathbf{z}^{init} \ \mathbf{1}]^T = H_{map}^{init} \cdot [\mathbf{x}^{map} \ \mathbf{y}^{map} \ \mathbf{z}^{map} \ \mathbf{1}]^T, \quad (1)$$

$$[\mathbf{u}^{init} \ \mathbf{v}^{init} \ \mathbf{1}]^T = K \cdot [\mathbf{x}^{init} \ \mathbf{y}^{init} \ \mathbf{z}^{init} \ \mathbf{1}]^T. \quad (2)$$

We keep track of indices of valid points in an array \mathbf{VI} . This is done by excluding indices of points whose projection lies behind or outside the image plane placed at H_{init} , as well as points marked as occluded by the occlusion estimation filter. Subsequently, we generate the LiDAR-image \mathcal{D} and project the map's points into a virtual image plane placed at

the ground truth pose H_{GT} . We then store the pixels' position of these projections as

$$\mathcal{D}_{\mathbf{u}_i^{init}, \mathbf{v}_i^{init}} = \mathbf{z}_i^{init}, \quad i \in \mathbf{VI}, \quad (3)$$

$$[\mathbf{u}^{GT} \ \mathbf{v}^{GT} \ \mathbf{1}]^T = K \cdot H_{map}^{GT} \cdot [\mathbf{x}^{map} \ \mathbf{y}^{map} \ \mathbf{z}^{map} \ \mathbf{1}]^T. \quad (4)$$

Finally, we compute the displacement ground truths ΔP by comparing the projections in the two image planes as

$$\Delta P_{\mathbf{u}_i^{init}, \mathbf{v}_i^{init}} = [\mathbf{u}_i^{GT} - \mathbf{u}_i^{init}, \mathbf{v}_i^{GT} - \mathbf{v}_i^{init}], \quad i \in \mathbf{VI}. \quad (5)$$

For every pixel $[u, v]$ without an associated 3D point, we set $\mathcal{D}_{u,v} = 0$ and $\Delta P_{u,v} = [0, 0]$. Moreover, we generate a mask of valid pixels as $mask_{u,v} = 1$ if $\mathcal{D}_{u,v} > 0$, 0 otherwise. We use a loss function that minimizes the sum of the regression component \mathcal{L}_{reg} and the smoothness component \mathcal{L}_{smooth} , to train our network. The regression loss defined in Equation (6) penalizes pixel displacements predicted by the network $\hat{\Delta P}$ that differs from their respective ground truth displacements ΔP on valid pixels. While the smoothness loss \mathcal{L}_{smooth} enforces the displacement of pixels without a ground truth to be similar to the ones in the neighboring pixels.

$$\mathcal{L}_{reg} = \frac{\sum_{u,v} \|\hat{\Delta P}_{u,v} - \Delta P_{u,v}\| \cdot mask_{u,v}}{\sum_{u,v} mask_{u,v}} \quad (6)$$

$$D_{smooth}(u, v) = \rho(\hat{\Delta P}_{u,v} - \hat{\Delta P}_{u+1,v}) + \rho(\hat{\Delta P}_{u,v} - \hat{\Delta P}_{u,v+1}) \quad (7)$$

$$\mathcal{L}_{smooth} = \frac{\sum_{u,v} D_{smooth}(u, v) \cdot (1 - mask_{u,v})}{\sum_{u,v} (1 - mask_{u,v})} \quad (8)$$

where ρ is the generalized Charbonnier function $\rho(x) = (x^2 + \epsilon^2)^\alpha$, $\epsilon = 10^{-9}$, $\alpha = 0.25$, as in [23].

B. Localization Step

Once CMRNet++ has been trained, we have the map, i.e., a set of 3D points \mathbf{P} whose coordinates are known, altogether with their projection in the LiDAR-image \mathcal{D} and a set \mathbf{p} of matching points in the RGB image that is predicted by the CNN given as

$$\mathbf{P}_i = [\mathbf{x}_i, \mathbf{y}_i, \mathbf{z}_i], \quad i \in \mathbf{VI}, \quad (9)$$

$$\mathbf{p}_i = [\mathbf{u}_i^{init}, \mathbf{v}_i^{init}] + \hat{\Delta P}_{\mathbf{u}_i^{init}, \mathbf{v}_i^{init}}, \quad i \in \mathbf{VI}. \quad (10)$$

Estimating the pose of the camera given a set of 2D-3D correspondences and the intrinsic matrix of the camera is known as the Perspective-n-Points (PnP) problem. To solve this problem, we used the EPnP algorithm [24] within a

RANdom SAMple Consensus (RANSAC) scheme [25], followed by an optimization method that minimizes the inliers' reprojection errors of the best RANSAC solution. We perform these operations using the OpenCV library [26].

C. Iterative Refinement

Similar to our previous work, we employ an iterative refinement technique in which we train different instances of CMRNet++ that are each specialized in handling different initial error ranges (in both translation and rotation) and then employ them for inference. During inference, we feed the RGB and LiDAR-image inputs to the network trained with the highest error range, and we generate a new LiDAR-image by projecting the map in the predicted pose. The latter is then fed to the second instance of CMRNet++ that is trained with a lower error range. This process can be repeated multiple times, iteratively improving the estimated localization accuracy.

D. Training Details

We train each instance of CMRNet++ from scratch for 300 epochs with a batch size of 40 using two NVIDIA Tesla P100. The weights of the network were updated with the ADAM optimizer with an initial learning rate of $1.5 \cdot 10^{-4}$ and a weight decay of $5 \cdot 10^{-6}$. We halved the learning rate after 20 and 40 epochs.

III. EXPERIMENTAL RESULTS

In this section, we first describe the datasets that we evaluate on, followed by the preprocessing steps that we employ, and then present the experimental results that validate our approach.

A. Datasets

To evaluate the localization performance of our CMRNet++ and to assess its generalization ability, we use three diverse autonomous driving datasets that cover different countries, different sensors, and different traffic conditions.

1) *KITTI*: The KITTI dataset [19] was recorded around the city of Karlsruhe, Germany. We use the *left* camera images from the odometry sequences 03, 05, 06, 07, 08 and 09 as the training set (total of 11 426 frames), and the sequence 00 as the validation set (4541 frames).

2) *Argoverse*: The recently introduced Argoverse dataset [20] was recorded in Miami and Pittsburgh. We used the images from the central forward facing camera (namely, *ring_front_center*) that provides 1920×1200 images at 30 fps. The images from *train1*, *train2* and *train3* splits of the “3D tracking dataset” were used as the training set (36 347 frames), and the *train4* split as the validation set (2741 frames).

3) *Lyft5*: The Lyft Level 5 AV dataset [21] was recorded in Palo Alto. We use the 1224×1024 images recorded from the front camera (namely, *CAM_FRONT*) from 10 selected urban scenes as validation set (1250 frames). We utilize the Lyft5 dataset to assess the generalization ability of our approach. We first train our CMRNet++ on KITTI and Argoverse, and then evaluate it on the Lyft5 dataset to assess the localization ability without any retraining. Therefore, this dataset was not included in the training set.

B. LiDAR-maps generation

In order to generate LiDAR-maps for the three aforementioned datasets, we first aggregate single scans at their respective ground truth position which is either provided by the dataset itself (Argoverse and Lyft5) or generated with a SLAM system [1] (KITTI). We then downsample the resulting maps at a resolution of 0.1 m with a voxel grid and we apply a statistical outlier removal technique to remove isolated points using the Open3D library [27]. Moreover, as we would like to have only static objects in the maps (*e.g.*, no pedestrians or cars), we remove dynamic objects by exploiting the 3D bounding boxes provided with Argoverse and Lyft5. Unfortunately, KITTI does not provide such bounding boxes for the odometry sequences, and therefore we could not remove dynamic objects for these sequences. In the future, we will leverage semantic segmentation techniques or 3D object detectors to remove them.

C. Training on multiple datasets

We train our CMRNet++ by combining training samples from KITTI and Argoverse datasets. Training a CNN on multiple diverse datasets creates certain challenges. First, the different cardinality of training sets of the two datasets (11 426 and 36 347, respectively) might lead the network to perform better on one dataset than the other. To overcome this problem, we randomly sampled a subset of Argoverse at the beginning of every epoch to have the same number of samples as KITTI. As the subset is sampled every epoch, the network will eventually process every sample from the Argoverse dataset.

Moreover, the two datasets have cameras with very different field of view and resolution. To address this issue, we reshape the images so they have the same resolution. One straightforward way to accomplish this would be to just crop the Argoverse images. However, this would yield images with a very narrow field of view, making the matching between the RGB and LiDAR-image increasingly difficult. Therefore, we first downsample the Argoverse images to half the original resolution (960×600), and then randomly crop both Argoverse and KITTI images to 960×320 pixels. We perform this random cropping at runtime during training in order to have different crop positions for the same image at different epochs. We generate both the LiDAR-image \mathcal{D} and the ground truth displacements ΔP at the original resolution, and then downsample and crop them accordingly. Moreover, we also halve the pixel displacements ΔP during the downsampling operation.

D. Initial pose sampling and data augmentation

We employ the iterative refinement approach presented in Section II-C by training three instances of CMRNet++. To simulate the initial pose H_{init} , we add uniform random noise to all components of the ground truth pose H_{GT} , independent for each sample. The range of the noise that we add to the first iteration is $[\pm 2 \text{ m}]$ for the translation and $[\pm 10^\circ]$ for the rotation. The maximum range for the second and third iteration are $[\pm 1 \text{ m}, \pm 2^\circ]$ and $[\pm 0.6 \text{ m}, \pm 1^\circ]$, respectively.

To improve the generalization ability of our approach, we employ a data augmentation scheme. First, we apply color

TABLE I
MEDIAN LOCALIZATION ERROR OF CMRNet++ ON KITTI, ARGOVERSE, AND LYFT5 DATASETS.

| | Training Max. Error Range | | KITTI Localization Error | | | Argoverse Localization Error | | | Lyft5 Localization Error | | |
|--------------|---------------------------|------------|--------------------------|----------------|----------|------------------------------|----------------|----------|--------------------------|----------------|----------|
| | Transl. [m] | Rot. [deg] | Transl. [m] | Rot. [deg] | Fail [%] | Transl. [m] | Rot. [deg] | Fail [%] | Transl. [m] | Rot. [deg] | Fail [%] |
| Initial pose | - | - | ≈ 1.97 | ≈ 9.83 | - | ≈ 1.97 | ≈ 9.83 | - | ≈ 1.97 | ≈ 9.83 | - |
| Iteration 1 | [-2, +2] | [-10, +10] | 0.55 | 1.46 | 2.18 | 0.80 | 1.55 | 6.24 | 1.32 | 2.13 | 10.56 |
| Iteration 2 | [-1, +1] | [-2, +2] | 0.22 | 0.77 | - | 0.34 | 0.58 | - | 0.79 | 1.28 | - |
| Iteration 3 | [-0.6, +0.6] | [-1, +1] | 0.14 | 0.43 | - | 0.25 | 0.45 | - | 0.70 | 1.18 | - |

The initial poses were randomly sampled from a uniform distribution in $[-2\text{m}, +2\text{m}]$, $[-10, +10]$, the first line shows the corresponding median values. Note that CMRNet++ was trained on KITTI and Argoverse, and only evaluated on Lyft5 to assess the generalization ability without any retraining.

TABLE II
COMPARISON WITH STATE-OF-THE-ART MONOCULAR APPROACHES.

| | Translation [m] | | | Rotation [deg] | | |
|--------------|-----------------|-------------|-------------|----------------|-------------|-------------|
| | Median | Mean | Std. Dev. | Median | Mean | Std. Dev. |
| Caseltz [14] | - | 0.30 | 0.11 | - | 1.65 | 0.91 |
| CMRNet [18] | 0.27 | 0.33 | 0.22 | 1.07 | 1.07 | 0.77 |
| CMRNet++ | 0.14 | 0.21 | 0.30 | 0.43 | 0.52 | 0.42 |

Localization errors comparison on the KITTI odometry sequence 00.

jittering to the images by randomly changing the contrast, saturation, and brightness. Subsequently, we randomly horizontally mirror the images, and we modify the camera calibration accordingly. We then randomly rotate the images in the range $[-5^\circ, 5^\circ]$. Finally, we transform the LiDAR point cloud to reflect these changes before generating the LiDAR-image.

To summarize, we train every instance of CMRNet++ as follows:

- Randomly draw a subset of the Argoverse dataset and shuffle it with samples from KITTI
- For every batch:
 - Apply data augmentation to the images \mathcal{I} and modify the camera matrices and the point clouds accordingly
 - Sample the initial poses H_{init}
 - Generate the LiDAR-images \mathcal{D} , the displacement ground truths ΔP and the masks $mask$
 - Downsample $\mathcal{I}, \mathcal{D}, \Delta P$ and $mask$ for the Argoverse samples in the batch
 - Crop $\mathcal{I}, \mathcal{D}, \Delta P$ and $mask$ to the resolution 960×320 .
 - Feed the batch $(\mathcal{I}, \mathcal{D})$ to CMRNet++, compute the loss, and update the weights
- Repeat for 300 epochs

E. Inference

During inference, we process one image at a time, and since the network architecture is fully convolutional, we do not resize the images of different datasets to have the same resolution. Therefore, we feed the whole image to CMRNet++ without any cropping. However, we still downsample the images of the Argoverse dataset to have a similar field of view as the images used for training. Once we have the set of 2D-3D correspondences predicted by the network, we apply PnP+RANSAC to estimate the pose of the camera *w.r.t.* the map, as detailed in Section II-B. We repeat this whole process three times using three specialized instances of CMRNet++ to iteratively refine the estimation.

F. Results

We evaluate the localization performance of CMRNet++ on the validation sets of the three datasets described in

Section III-A. It is important to note that all the validation sets are geographically separated from the training set; thus, we evaluate CMRNet++ in places that were never seen during the training phase. Moreover, as the Lyft5 dataset was not used for training, we evaluate the performance of our approach in a completely different city and on data gathered with different sensors. The median localization errors for the three iterations of the iterative refinement technique are reported in Table I. Furthermore, videos showing qualitative results are available at <http://rl.uni-freiburg.de/research/vloc-in-lidar>. We also provide comparisons of our proposed CMRNet++ with CMRNet and the approach of [14] in Table II. The results demonstrate that CMRNet++ outperforms the other methods on the sequence 00 of the KITTI dataset. Although [14] achieves a lower standard deviation for the translation component, it further exploits tracking and temporal filtering which our approach does not. Therefore, the variance of our method can be further lowered by incorporating such techniques.

As opposed to CMRNet, CMRNet++ can fail to localize an image. This occurs in the first iteration when more than half of the matches predicted by the network are wrong, and therefore PnP+RANSAC might estimate an incorrect solution. We believe that the root cause of this issue is the matching of pixels on the ground plane. Due to the uniform appearance of the road surface, it is nearly impossible to recognize the exact pixel that matches a specific 3D point on the road. To identify such cases, we mark the samples as *failed* for which the estimated pose after the first iteration is farther than four meters from H_{init} . Failed samples are not fed into the second and third iterations. The percentage of failed samples for each validation set is also reported in Table I.

IV. CONCLUSIONS

In this paper we proposed CMRNet++, a novel CNN-based approach for monocular localization in LiDAR-maps. We designed CMRNet++ to be independent of both the map and camera intrinsics. To the best of our knowledge, CMRNet++ is the first Deep Neural Network (DNN)-based approach for pose regression that generalizes to new environments without any retraining.

We demonstrated the performance our approach on KITTI, Argoverse, and Lyft Level 5 datasets in which our CMRNet++ localizes a single RGB image in unseen places with a median error as low as 0.14m and 0.43° , outperforming other state-of-the-art approaches. Moreover, results on the Lyft Level 5 dataset that was excluded from training show that CMRNet++ is able to effectively generalize to previously unseen environments as well as to different sensors.

ACKNOWLEDGMENTS

This work was partly funded by the European Union's Horizon 2020 research and innovation program under grant agreement No 871449-OpenDR, by the Federal Ministry of Education and Research (BMBF) of Germany under SORTIE. The authors would like to thank Pietro Colombo for assistance in making the video.

REFERENCES

- [1] R. Kümmerle, M. Ruhnke, B. Steder, C. Stachniss, and W. Burgard, "Autonomous robot navigation in highly populated pedestrian zones," *Journal of Field Robotics*, vol. 32, no. 4, pp. 565–589, 2015.
- [2] J. Behley and C. Stachniss, "Efficient surfel-based slam using 3d laser range data in urban environments," in *Robotics: Science and Systems (RSS)*, 2018.
- [3] T. Sattler, W. Maddern, C. Toft, A. Torii, L. Hammarstrand, E. Stenborg, D. Safari, M. Okutomi, M. Pollefeys, J. Sivic, *et al.*, "Benchmarking 6dof outdoor visual localization in changing conditions," in *IEEE Conference on Computer Vision and Pattern Recognition (CVPR)*, 2018, pp. 8601–8610.
- [4] T. Sattler, B. Leibe, and L. Kobbelt, "Efficient & effective prioritized matching for large-scale image-based localization," *IEEE transactions on pattern analysis and machine intelligence*, vol. 39, no. 9, pp. 1744–1756, 2016.
- [5] F. Boniardi, A. Valada, R. Mohan, T. Caselitz, and W. Burgard, "Robot localization in floor plans using a room layout edge extraction network," *arXiv preprint arXiv:1903.01804*, 2019.
- [6] A. Kendall, M. Grimes, and R. Cipolla, "PoseNet: A convolutional network for real-time 6-DOF camera relocalization," in *IEEE International Conference on Computer Vision (ICCV)*, December 2015.
- [7] N. Radwan, A. Valada, and W. Burgard, "VLocNet++: deep multitask learning for semantic visual localization and odometry," *IEEE Robotics and Automation Letters*, vol. 3, no. 4, pp. 4407–4414, 2018.
- [8] A. Valada, N. Radwan, and W. Burgard, "Deep auxiliary learning for visual localization and odometry," in *2018 IEEE international conference on robotics and automation (ICRA)*, 2018, pp. 6939–6946.
- [9] E. Brachmann and C. Rother, "Learning less is more - 6D camera localization via 3D surface regression," in *The IEEE Conference on Computer Vision and Pattern Recognition (CVPR)*, June 2018.
- [10] A. Valada, N. Radwan, and W. Burgard, "Incorporating semantic and geometric priors in deep pose regression," in *Workshop on Learning and Inference in Robotics: Integrating Structure, Priors and Models at Robotics: Science and Systems (RSS)*, 2018.
- [11] J. Shotton, B. Glocker, C. Zach, S. Izadi, A. Criminisi, and A. Fitzgibbon, "Scene coordinate regression forests for camera relocalization in RGB-D images," in *IEEE Computer Vision and Pattern Recognition (CVPR)*, June 2013.
- [12] T. Cavallari, S. Golodetz, N. A. Lord, J. Valentin, L. Di Stefano, and P. H. Torr, "On-the-fly adaptation of regression forests for online camera relocalisation," in *IEEE Conference on Computer Vision and Pattern Recognition (CVPR)*, 2017, pp. 4457–4466.
- [13] T. Sattler, Q. Zhou, M. Pollefeys, and L. Leal-Taixe, "Understanding the limitations of cnn-based absolute camera pose regression," in *IEEE Conference on Computer Vision and Pattern Recognition (CVPR)*, 2019, pp. 3302–3312.
- [14] T. Caselitz, B. Steder, M. Ruhnke, and W. Burgard, "Monocular camera localization in 3d lidar maps," in *IEEE/RSJ Intelligent Robots and Systems (IROS)*, Oct 2016.
- [15] M. Sun, S. Yang, and H. Liu, "Scale-aware camera localization in 3d lidar maps with a monocular visual odometry," *Computer Animation and Virtual Worlds*, vol. 30, no. 3-4, p. e1879, 2019.
- [16] R. W. Wolcott and R. M. Eustice, "Visual localization within LIDAR maps for automated urban driving," in *IEEE/RSJ Intelligent Robots and Systems (IROS)*, Sep. 2014.
- [17] P. Neubert, S. Schubert, and P. Protzel, "Sampling-based methods for visual navigation in 3d maps by synthesizing depth images," in *2017 IEEE/RSJ International Conference on Intelligent Robots and Systems (IROS)*. IEEE, 2017, pp. 2492–2498.
- [18] D. Cattaneo, M. Vaghi, A. L. Ballardini, S. Fontana, D. G. Sorrenti, and W. Burgard, "CMRNet: Camera to LiDAR-Map registration," in *2019 IEEE Intelligent Transportation Systems Conference (ITSC)*, 2019, pp. 1283–1289.
- [19] A. Geiger, P. Lenz, C. Stiller, and R. Urtasun, "Vision meets robotics: The kitti dataset," *The International Journal of Robotics Research*, vol. 32, no. 11, pp. 1231–1237, 2013.
- [20] M.-F. Chang, J. W. Lambert, P. Sangkloy, J. Singh, S. Bak, A. Hartnett, D. Wang, P. Carr, S. Lucey, D. Ramanan, and J. Hays, "Argoverse: 3d tracking and forecasting with rich maps," in *Conference on Computer Vision and Pattern Recognition (CVPR)*, 2019.
- [21] R. Kesten, M. Usman, J. Houston, T. Pandya, K. Nadhamuni, A. Ferreira, M. Yuan, B. Low, A. Jain, P. Ondruska, S. Omari, S. Shah, A. Kulkarni, A. Kazakova, C. Tao, L. Platinsky, W. Jiang, and V. Shet, "Lyft level 5 av dataset 2019," <https://level5.lyft.com/dataset/>, 2019.
- [22] D. Sun, X. Yang, M.-Y. Liu, and J. Kautz, "PWC-Net: CNNs for optical flow using pyramid, warping, and cost volume," in *The IEEE Conference on Computer Vision and Pattern Recognition (CVPR)*, June 2018.
- [23] J. J. Yu, A. W. Harley, and K. G. Derpanis, "Back to basics: Unsupervised learning of optical flow via brightness constancy and motion smoothness," in *Computer Vision – ECCV 2016 Workshops*, G. Hua and H. Jégou, Eds. Cham: Springer International Publishing, 2016, pp. 3–10.
- [24] V. Lepetit, F. Moreno-Noguer, and P. Fua, "EPnP: An accurate o(n) solution to the PnP problem," *International Journal of Computer Vision*, vol. 81, no. 2, p. 155, 2009.
- [25] M. A. Fischler and R. C. Bolles, "Random sample consensus: a paradigm for model fitting with applications to image analysis and automated cartography," *Communications of the ACM*, vol. 24, no. 6, pp. 381–395, 1981.
- [26] G. Bradski, "The OpenCV Library," *Dr. Dobbs's Journal of Software Tools*, 2000.
- [27] Q.-Y. Zhou, J. Park, and V. Koltun, "Open3D: A modern library for 3D data processing," *arXiv:1801.09847*, 2018.